Supplemental Information for

# Gravimetrically Measured Water Content of Filter Sampled Fine Particulate Matter at Low Relative Humidity: Insight from the Surface Particulate Matter Network (SPARTAN)

Author list: Christopher R. Oxford[1]*, Haihui Zhu[1,2], Maya Mehrotra[1], Xuan Liu[1,3], Yuxuan Ren[1], Maya Arnott[1], Isaac Abionum Adimula[4], Taiye Benjamin Ajibolataiye[4], Clement Akoshile[4], Omar Amador-Munoz[5], Araya Asfaw[6], Rachel Ying-Wen Chang[7], Sagnik Dey[8,9], Ann M. Dillner[10], David J. Diner[11], Connor J. Flynn[12], Diana Francis[13], Paterne Gahungu[14], Rebecca M. Garland[15,16], Michel Grutter[5], Sina Hasheminassab[11], Fahad Imam[8], Jhoon Kim[17], Kristy Langerman[18], Pei-Chen Lee[19], Puji Lestari[20], Po-Hsiung Lin[21], S. Marcela Loria-Salazar[12], Tesfaye Mamo[22], Olga L. Mayol-Bracero[23], Mogesh Naidoo[15], Narendra Nelli[13], Sang Seo Park[24], Abdus Salam[25], Bighnaraj Sarangi[23], Trailokya Saud[26] , Robyn Schofield[27], Yoav Schechner[28] Sachchida N. Tripathi[29], Emily K. West[12], Eli Windwer[30], Ming-Tsang Wu[31,32], Qiang Zhang[33], Michael Brauer[34], Yinon Rudich[30], Jay R. Turner[1], and Randall V. Martin[1]

[1] Department of Energy, Environmental & Chemical Engineering, Washington University in St. Louis, St. Louis, Missouri 63130, United States

[2] Department of Atmospheric Science, Colorado State University, Fort Collins, Colorado 80521, United States

[3] Scripps Institution of Oceanography, University of California San Diego, San Diego, California 92093, United States

[4] Department of Physics, University of Ilorin, Ilorin, 240003, Nigeria

[5] Instituto de Ciencias de la Atmósfera y Cambio Climático, Universidad Nacional Autónoma de México, Mexico City, 04510, Mexico

[6] Institute of Geophysics and Space Science, Addis Ababa University, Addis Ababa,1176, Ethiopia

[7] Department of Physics and Atmospheric Science, Dalhousie University, Halifax, Nova Scotia B3H 4R2, Canada

[8] Indian Institute of Technology Delhi, Hauz Khas, New Delhi, India 110016

[9] Adjunct Faculty, Department of Health, Management and Policy, Korea University, Seoul, South Korea

[10] Air Quality Research Center, University of California Davis, Davis, CA, USA

[11] Jet Propulsion Laboratory, California Institute of Technology, Pasadena, California, United States

[12] School of Meteorology, University of Oklahoma, Norman, Oklahoma, United States

[13] Environmental and Geophysical Sciences Lab, Earth Science Department, Khalifa University, Abu Dhabi, 127788, United Arab Emirates

[14] Institute of Applied Statistics, University of Burundi, Bujumbura, BP1550, Burundi

[15] Council for Scientific and Industrial Research, Pretoria, 0001, South Africa

[16] Department of Geography, Geo-Informatics and Meteorology, University of Pretoria, Pretoria, 0002, South Africa

[17] Department of Atmospheric Sciences, Yonsei University, Seoul, 03722, Republic of Korea

[18] Department of Geography, Environmental Management and Energy Studies, University of Johannesburg, Johannesburg, 2006, South Africa

[19] Department of Public Health, National Cheng Kung University, Tainan, 701, Taiwan

[20] Faculty of Civil and Environmental Engineering, Bandung Institute of Technology, Bandung, 40132, Indonesia

[21] Department of Atmospheric Sciences, National Taiwan University, Taipei, Taiwan

[22] Department of Physics, Addis Ababa University, Addis Ababa, Ethiopia

[23] Department of Environmental Science, University of Puerto Rico, Puerto Rico, 00931, United States

[24] Department of Urban and Environmental Engineering, Ulsan National Institute of Science and Technology, Ulsan, 44919, Republic of Korea

[25] Department of Chemistry, University of Dhaka, Dhaka, 1000, Bangladesh

[26] National Aerosol Facility, Indian Institute of Technology Kanpur, Kanpur, 208016, India

[27] School of Geography, Earth and Atmospheric Sciences, University of Melbourne, Melbourne, 3010, Australia

[28] Department of Electrical Engineering, Technion Israel Institute of Technology, Haifa, 3200003, Israel

[29] Kotak School of Sustainability, Indian Institute of Technology Kanpur, Kanpur, 208016, India

[30] Department of Earth and Planetary Sciences, Weizmann Institute of Science, Rehovot, 76100, Israel

[31] Department of Family Medicine, Kaohsiung Medical University Hospital, Kaohsiung Medical University, Kaohsiung, 807, Taiwan

[32] PhD Program in Environmental and Occupational Medicine, Kaohsiung Medical University, Kaohsiung, 807, Taiwan

[33] School of Environment, Tsinghua University, Beijing, 100084, China

[34] School of Population and Public Health, University of British Columbia, Vancouver, British Columbia V6T 1Z3, Canada

Table S1. Site and host institutes of the SPARTAN sites used in this study.

| Site City | Host Institute | Latitude | Longitude |
|---|---|---|---|
| Abu Dhabi | Masdar Institute | 24.44 | 54.62 |
| Addis Ababa | Addis Ababa University | 9.01 | 38.82 |
| Bandung | Bandung Institute of Technology | -6.89 | 107.61 |
| Beijing | Tsinghua University | 40.00 | 116.33 |
| Bujumbura | University of Burundi | -3.38 | 29.38 |
| Delhi | Indian Institute of Technology Delhi | 28.54 | 77.19 |
| Dhaka | Dhaka University | 23.73 | 90.40 |
| Fajardo | Cabezas de San Juan Nature Reserve | 18.38 | -65.62 |
| Haifa | Technion Israel Institute of Technology | 32.78 | 35.02 |
| Halifax | Dalhousie University | 44.64 | -63.59 |
| Ilorin | Ilorin University | 8.48 | 4.67 |
| Johannesburg | University of Johannesburg | -26.18 | 28 |
| Kanpur | Indian Institute of Technology Kanpur | 26.51 | 80.23 |
| Kaohsiung | Kaohsiung Medical University | 22.65 | 120.31 |
| Melbourne | The University of Melbourne | -37.8 | 144.97 |
| Mexico City | Universidad Nacional Autónoma de México | 19.33 | -99.18 |
| Norman | University of Oklahoma | 35.18 | -97.44 |
| Pasadena | Jet Propulsion Laboratory | 34.20 | -118.17 |
| Pretoria | Council for Scientific and Industrial Research | -25.76 | 28.28 |
| Rehovot | Weizmann Institute | 31.91 | 34.81 |
| Seoul | Yonsei University | 37.56 | 126.93 |
| Sherbrooke | Sherbrooke University | 45.38 | -71.93 |
| Taipei | National Taiwan University | 25.04 | 121.50 |
| Ulsan | Ulsan National Institute of Science and Technology | 35.58 | 129.19 |

Supplemental Text S1: Acceptance of new polytetrafluoroethylene (PTFE) filters

Acceptance testing is performed on every box of PTFE filters by measuring the contamination level on a select group of five new filters from the box of 100. The 5 filters are pre-weighed by the Measurement Technology Laboratories AH500 system to confirm the barcodes are legible and the filters have nominal weights between 90 and 100 mg. After weighing, we measure each filter using XRF. To be accepted all XRF measurements must be less than the mean plus three times the standard deviation determined from 100 laboratory blank filters selected from multiple boxes for all measured species. After passing XRF, two of the five filters are extracted using procedures defined in section 2.2. We then measure the extract using Ion Chromatography. All species in the extract must be below mean plus 3 times standard deviation determined from 100 laboratory blank filters from multiple boxes. The remaining three unextracted filters are used as lab blanks for measurements at University of California Davis.

Table S2. The beginning and latest samples along with the protocol used during the sample period. Hours is the number of sampling hours per sample filter.

| Site city | Start Date | Latest Date | Protocol | Hours per sample | Notes: |
|---|---|---|---|---|---|
| Abu Dhabi | 7/27/2020 | 7/21/2024 | SPARTAN | 24 | |
| | 7/31/2024 | 9/22/2024 | SPARTAN | 12 | |
| Addis Ababa | 12/7/2022 | 5/13/2024 | MAIA | 24 | |
| Bandung | 12/31/2019 | 7/11/2021 | SPARTAN | 24 | |
| Beijing | 3/24/2020 | 8/27/2022 | SPARTAN | 24 | |
| | 8/30/2022 | 6/16/2024 | MAIA | 24 | |
| | 6/26/2024 | 8/18/2024 | SPARTAN | 24 | |
| Bujumbura | 12/9/2022 | 8/9/2024 | SPARTAN | 24 | |
| Delhi | 3/5/2024 | 5/13/2024 | MAIA | 12 | |
| Dhaka | 8/11/2020 | 7/17/2023 | SPARTAN | 24 | Contains period of special protocol[a] |
| | 8/15/2023 | 6/2/2024 | SPARTAN | 12 | |
| Fajardo | 3/18/2021 | 2/7/2024 | SPARTAN | 24 | |
| Haifa | 2/16/2022 | 4/11/2023 | MAIA | 24 | |
| Halifax | 1/14/2020 | 2/12/2024 | SPARTAN | 48 | |
| Ilorin | 6/22/2020 | 12/1/2021 | SPARTAN | 24 | |
| Johannesburg | 4/10/2022 | 1/12/2024 | MAIA | 24 | |
| | 1/23/2024 | 7/26/2024 | SPARTAN | 24 | |
| Kanpur | 7/14/2021 | 5/24/2022 | SPARTAN | 24 | |
| Kaohsiung | 8/20/2022 | 1/25/2024 | MAIA | 24 | |
| | 2/21/2024 | 7/26/2024 | SPARTAN | 24 | |
| Melbourne | 8/9/2022 | 5/20/2024 | SPARTAN | 24 | |
| Mexico City | 2/26/2021 | 6/9/2024 | SPARTAN | 24 | |
| Norman | 6/28/2023 | 3/18/2024 | SPARTAN | 24 | |
| Pasadena | 11/9/2021 | 8/23/2024 | MAIA | 24 | Contains period of special protocol[b] |
| Pretoria | 10/22/2020 | 4/5/2021 | SPARTAN | 24 | |
| | 4/15/2021 | 1/24/2024 | MAIA | 24 | |
| | 5/17/2024 | 7/1/2024 | SPARTAN | 24 | |
| Rehovot | 7/2/2020 | 4/13/2021 | SPARTAN | 24 | |
| | 11/5/2021 | 6/7/2023 | MAIA | 24 | |
| Seoul | 9/11/2020 | 1/8/2024 | SPARTAN | 24 | |
| Sherbrooke | 3/10/2020 | 8/22/2024 | SPARTAN | 48 | |
| Taipei | 1/27/2022 | 2/9/2024 | MAIA | 24 | |
| | 2/18/2024 | 8/4/2024 | SPARTAN | 24 | |
| Ulsan | 10/28/2021 | 8/22/2024 | SPARTAN | 24 | |

[a] – this sampling period contains co-located (2 sampling stations), continuous samples from June and July 2023. [b] – this sampling period contains pseudo co-located (1 sampling station) samples from March to August 2024.

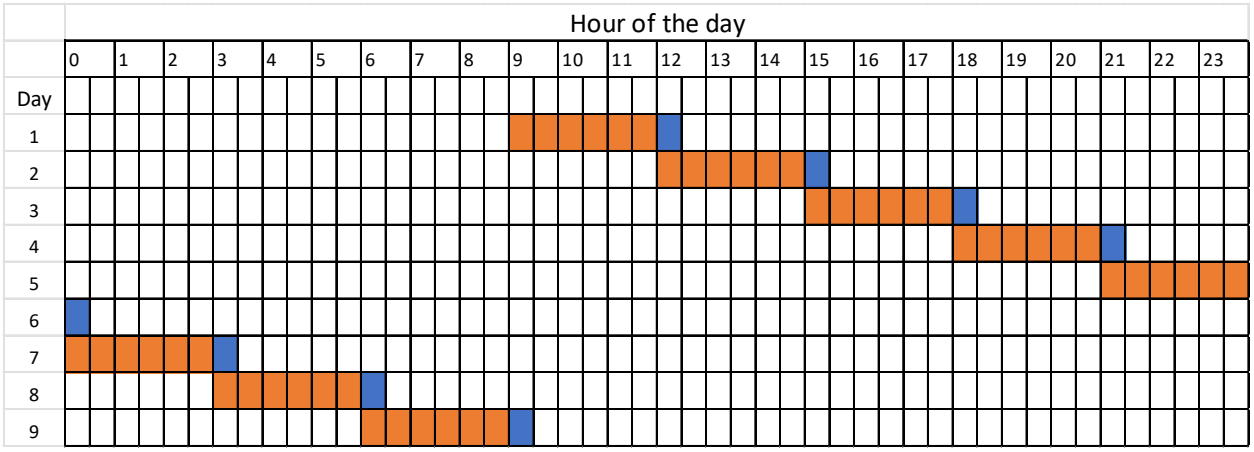


Figure S1. Example SPARTAN 9-day sampling protocol. A 24-hour diurnal cycle is collected over the course of 9 days. Orange represents $PM_{2.5}$ sampling; blue represents $PM_{10}$ sampling. In this example, a single $PM_{2.5}$ filter is sampled for 24 hours. The $PM_{10}$ filter is sampled for 4 hours during each of 6 $PM_{2.5}$ filters in a cartridge.

## Supplemental Text S2: Fourier Transfer Infrared (FTIR) spectroscopy

All filter samples were scanned 512 times by an FTIR instrument from 4000 to 420 $cm^{-1}$ in transmission mode. This process began with purging the measurement chamber with dry air without carbon dioxide. The resulting scan was converted to absorbance using the zero-reference signal. The subsequent spectra was then baseline corrected using multiple lab blank filters from the same lot. A calibration model of elemental carbon (EC) and organic carbon (OC) created using 22 IMPROVE sites with parallel measurements of EC and OC using Thermal-Optical-Reflectance (TOR) (Dillner and Takahama, 2015a, b; Reggente et al., 2016) was used to quantify the mass of the EC and OC species.

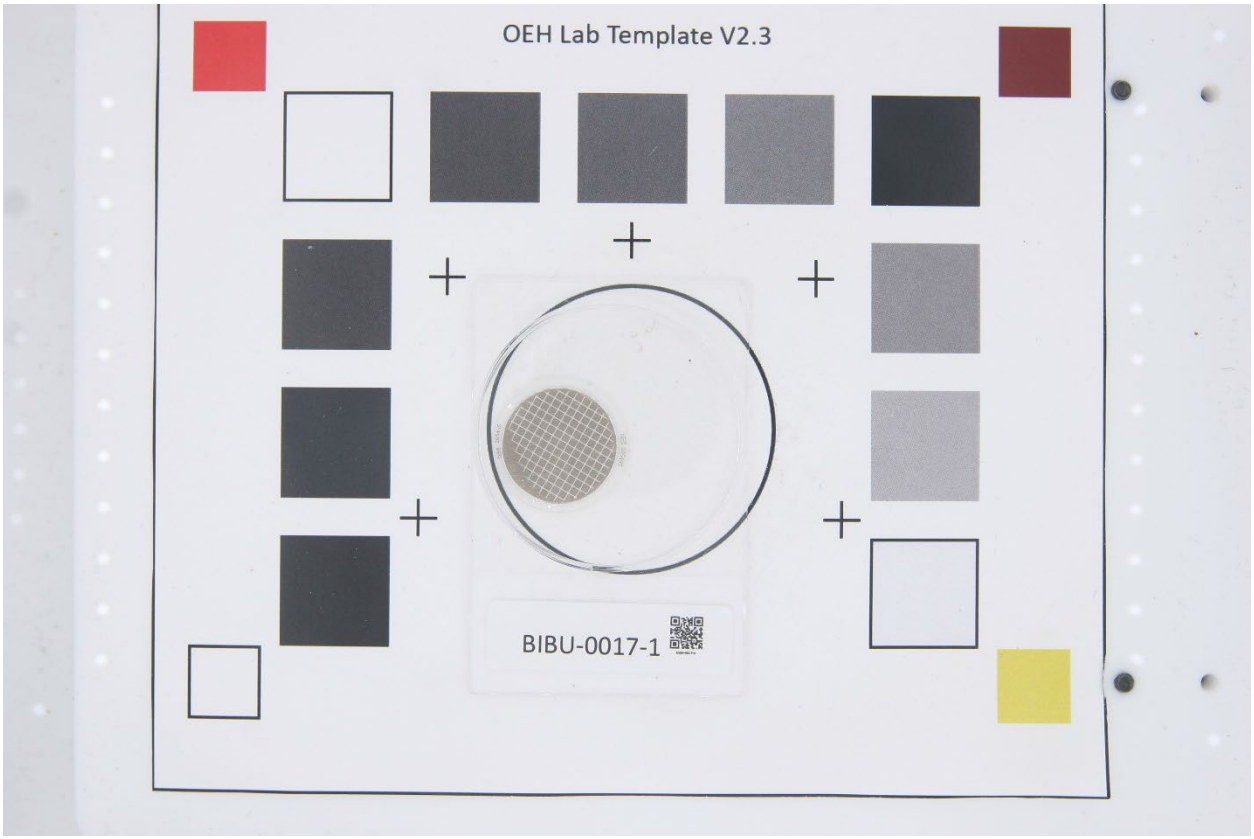


Figure S2. An example individual photograph on the calibrated background as mentioned in Section 2.2. This filter is a member of the 12 filters in the Bujumbura proxy sample.

## Supplemental Text S3: UV-Vis spectroscopy

All filter samples were scanned with a PerkinElmer LAMBDA 35 UV-Vis spectrophotometer with an integrating sphere installed between two sample holders as described by Zhong and Jang (2011). The transmittance and reflectance were both measured with the sample facing towards the light source. The transmittance was measured by placing the sample in between the light source and the sphere with the downstream sample holder containing a white standard. The reflectance was measured by placing the sample in the downstream sample holder with an empty upstream sample holder. The two measurement values were then placed into an empirical relationship to determine Mass Absorption Cross section (MAC) (Pandey et al., 2019). The empirical relationship was based upon 90 measurements of various aerosols with a Single Scattering Albedos ranging from 0.25 to 0.99.

## Supplemental Text S4: Labware cleaning procedures

The cleaning process for the scintillation vials began with 24 hours in a bath of 1% nitric acid. After 24 hours in the acid bath, the vials were rinsed with deionized water 3 times and 1 time with ACS grade methanol. The vials were then lightly tamped on a surface until all standing liquid was removed from the vial. The vial then dried inverted overnight. After drying, the vials were wrapped in aluminum foil and baked in an oven at 500 °C for 5 hours. After cooling, the vials were stored for future use. All syringes were cleaned by submersion in ACS grade methanol once, and then by submersion in deionized water 3 times. The syringes were then lightly tamped until all visible water was removed and then left inverted to dry. The syringes were then reassembled and wrapped with aluminum foil until future use. The opaque Nalgene vials were also submerged in methanol once and submerged in deionized water 3 times. They were tamped until all water was removed and placed inverted to dry. The syringe filters are rinsed before use with 8 to 10 ml of deionized water immediately prior to use.

## Supplemental Text S5: Choice of linear model for evaporation.

Equation S1 describes the evaporation of a single particle.

$$MFR = \left(1 - \frac{2D}{\rho_p {r_p}^2} C^* t\right)^{(3/2)} \quad \text{(S1)}$$

where $MFR$ is the mass fraction remaining, $D$ is diffusivity of the evaporating species in the gas phase (assumed $10^{-5}$ $cm^2/s$), $\rho_p$ is the particle density (assumed 1.2 $g/cm^3$), $r_p$ is the initial radius of the particle (assumed 400 nm), $C^*$ is the mass concentration of the gas phase in equilibrium at the particle surface, and $t$ is time.

Figure S3 shows the results when Equation S1 is fit to Beijing data, which is the fastest evaporating sample in the study. In the fitting process, C* was used as the fitted parameter. The resulting C* value is 2.67 $\mu g/m^3$, which is similar to other atmospheric aerosols (Donahue et al., 2006). The left panel shows that the evaporation curve is not linear over timescales of thousands of hours. However, the right panel shows that over the time range of the experiment, the evaporation model is approximately linear.

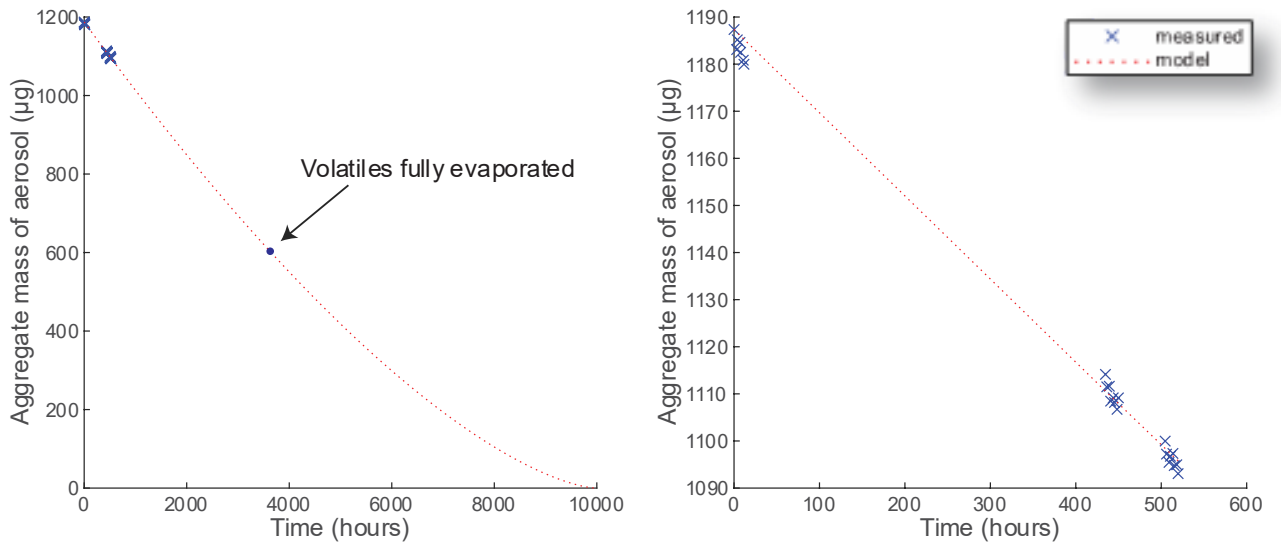


Figure S3. Equation S1 fit to the Beijing evaporation data. The left panel displays evaporation of the entire particle. However, the volatiles should be fully evaporated by 3629 hours using this model. The right panel highlights the first 600 hours of that evaporation.

Supplemental Figures displaying the raw measurements from the remaining sites

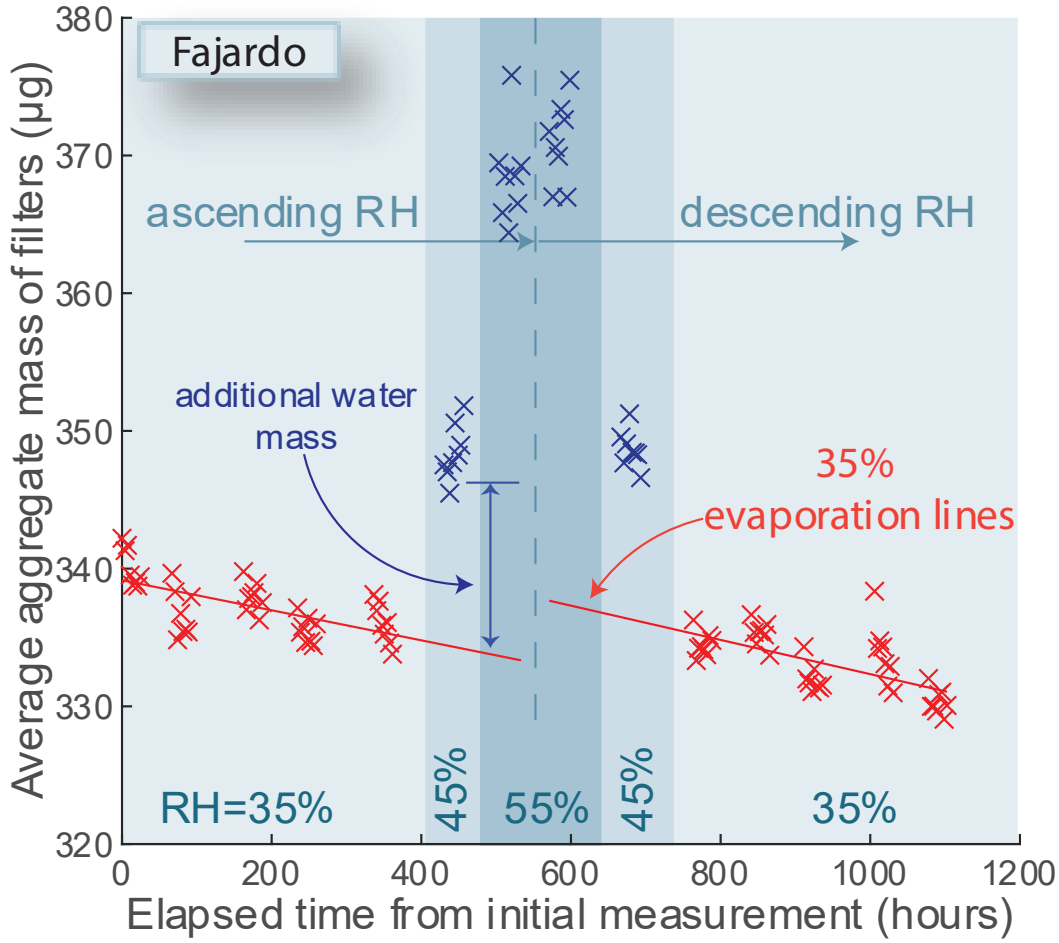


Figure S4. The RH-gravimetric response of filters from Fajardo, Puerto Rico. The red evaporation lines connect the measurements at 35% relative humidity (red X's). The change in water mass is the difference between the mass measurements at elevated relative humidity (blue X's) and the red evaporation line. Shading in the plot represents the different relative humidities in the experiment.

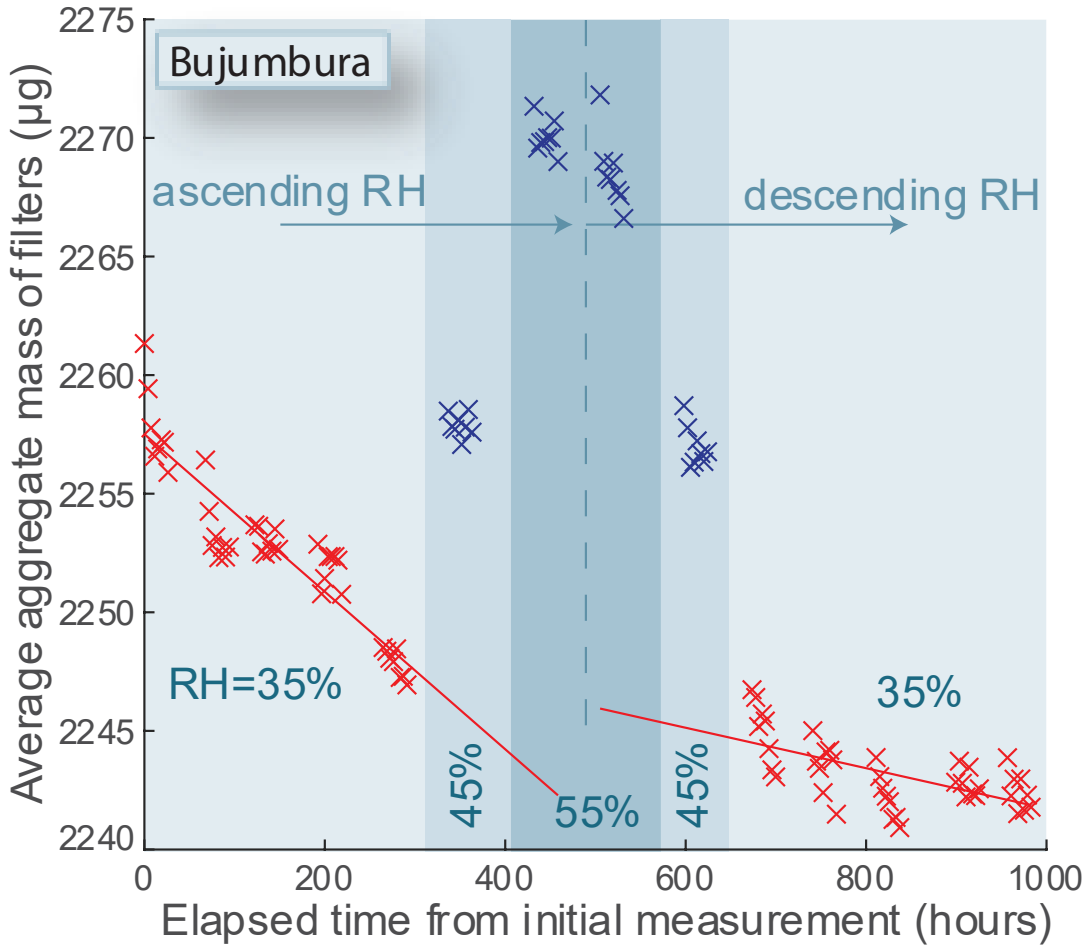


Figure S5. The RH-gravimetric response of filters from Bujumbura, Burundi. The red evaporation lines connect the measurements at 35% relative humidity (red X's). The change in water mass is the difference between the mass measurements at elevated relative humidity (blue X's) and the red evaporation line. Shading in the plot represents the different relative humidities in the experiment.

Supplemental Text S6: Calculation of uncertainty from the original datasets

We assumed that two different sources of uncertainty impact the measurements: subgroup uncertainty (short-term) and group uncertainty (long-term). We characterized both uncertainties and then used those two uncertainties to deviate the original dataset. This new faux dataset was used with the original scripts to calculate the variables of interest.

The subgroup uncertainty was calculated using all subgroups in the dataset. The group average was subtracted from the subgroup to calculate a subgroup deviation

(deviation from the group mean). Then each subgroup deviation was placed in temporal measurement order: all first subgroups deviations are grouped together, all second subgroup deviations are grouped together, up to the eighth subgroup creating distributions of all 8 subgroups. Assuming normality, we calculated the average and standard deviation for each of the eight subgroups while excluding outliers.

The group uncertainty is calculated using the 35% RH data only. We calculated the deviations between each group average and the fitted 35% evaporation line. This generated a set of group deviations which again is assumed normal. We then calculated the group average and group standard deviation.

To generate a new dataset, the group average from the original dataset was calculated (for all RH in the dataset). Then each group average was deviated using the group deviation distribution. Lastly, each subgroup was calculated by deviating the faux group average using the 8 subgroup distributions. This generated a faux dataset. An example is shown in Figure S6.

We generated a faux dataset for each of the three proxy samples (Abu Dhabi, Fajardo, and Bujumbura) and then fed them through all scripts to determine the water content for each growth category. We created 10,000 groups of three faux datasets which were used to calculate uncertainty in the water content of each growth category.

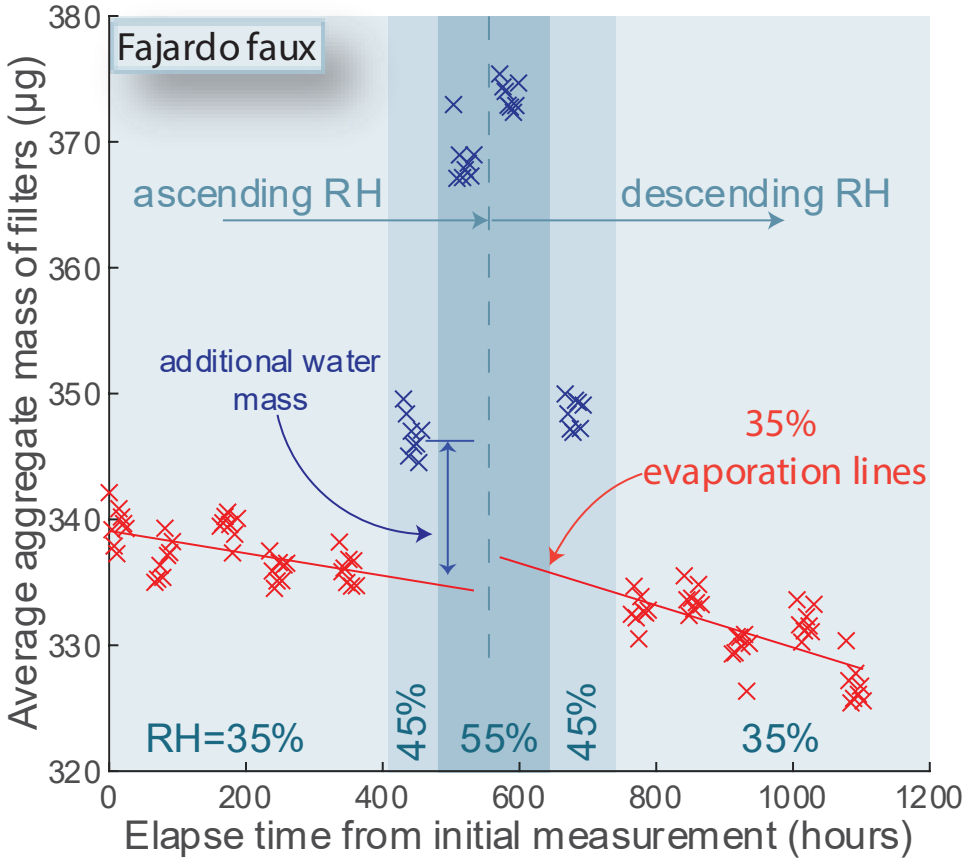


Figure S6. A faux dataset generated from the original Fajardo dataset shown in Figure S5.

Table S3. Predicted water content at 40% RH using the solved water categories compared to the measurements by Mcinnes et al. (1996) at the same RH.

| Growth Category | This study prediction Mean (95% CI) | Mcinnes et al. (1996) measurements Mean (Range) |
|---|---|---|
| High Growth (NaCl) | 20.3% (14.9-30.5%) | 26.4% (19.9-32.6%) (lab sea salt) |
| Med Growth (A-N-S-K) | 4.76% (3.72-5.03%) | 3.76% (0-8.1%) (ammonium sulfate) |

Table S4. Average composition in μg/m$^3$ of the samples used in the study.

| Site | $PM_{2.5}$ | BC | TEO | Dust | $Na^+$ | $NO_3^-$ | $NH_4^+$ | $SO_4^{2-}$ | PBW | $Cl^-$ | $K^+$ | RM |
|---|---|---|---|---|---|---|---|---|---|---|---|---|
| Abu Dhabi | 32.93 | 2.62 | 0.14 | 13.01 | 0.28 | 0.10 | 3.20 | 13.03 | 0.74 | 0.02 | 0.04 | -0.22 |
| Melbourne | 4.79 | 0.52 | 0.01 | 0.56 | 0.13 | 0.00 | 0.02 | 0.64 | 0.10 | 0.09 | 0.00 | 2.71 |
| Dhaka | 37.52 | 4.61 | 6.61 | 6.53 | 0.10 | 0.17 | 0.74 | 6.08 | 0.55 | 0.58 | 0.41 | 11.15 |
| Bujumbura | 30.67 | 3.68 | 0.12 | 2.06 | 0.04 | 0.00 | 0.17 | 1.61 | 0.36 | 0.01 | 0.95 | 21.67 |
| Halifax | 3.11 | 0.23 | 0.01 | 0.25 | 0.01 | 0.00 | 0.01 | 0.50 | 0.05 | 0.03 | 0.01 | 1.99 |
| Sherbrooke | 4.64 | 0.37 | 0.01 | 0.41 | 0.00 | 0.05 | 0.06 | 0.59 | 0.06 | 0.00 | 0.00 | 3.09 |
| Beijing | 25.49 | 1.45 | 0.18 | 4.37 | 0.05 | 4.56 | 2.19 | 3.88 | 0.56 | 0.03 | 0.22 | 8.01 |
| Addis Ababa | 21.66 | 4.71 | 0.07 | 5.07 | 0.01 | 0.00 | 0.44 | 2.07 | 0.21 | 0.01 | 0.21 | 8.86 |
| Bandung | 27.30 | 3.40 | 0.19 | 1.34 | 0.00 | 0.00 | 1.64 | 5.24 | 0.46 | 0.00 | 0.27 | 14.75 |
| Haifa | 12.85 | 0.81 | 0.05 | 3.30 | 0.10 | 0.03 | 1.31 | 4.08 | 0.28 | 0.03 | 0.00 | 2.85 |
| Rehovot | 14.21 | 1.25 | 0.07 | 3.73 | 0.05 | 0.16 | 1.21 | 3.94 | 0.27 | 0.02 | 0.00 | 3.51 |
| Delhi | 55.40 | 5.98 | 1.00 | 9.95 | 0.38 | 0.47 | 2.43 | 7.95 | 1.25 | 2.40 | 1.86 | 21.74 |
| Kanpur | 43.88 | 4.24 | 0.56 | 10.83 | 0.14 | 0.43 | 1.93 | 7.84 | 0.68 | 0.04 | 1.09 | 16.08 |
| Seoul | 18.14 | 1.19 | 0.11 | 2.37 | 0.00 | 2.03 | 1.70 | 2.99 | 0.36 | 0.00 | 0.04 | 7.36 |
| Ulsan | 12.65 | 0.76 | 0.13 | 2.01 | 0.06 | 0.62 | 1.15 | 2.48 | 0.25 | 0.05 | 0.01 | 5.13 |
| Mexico City | 15.51 | 2.15 | 0.08 | 1.26 | 0.00 | 0.00 | 1.10 | 3.17 | 0.26 | 0.00 | 0.09 | 7.40 |
| Ilorin | 25.63 | 3.06 | 1.01 | 11.22 | 0.00 | 0.00 | 0.08 | 1.56 | 0.19 | 0.11 | 0.42 | 7.99 |
| Fajardo | 6.49 | 0.10 | 0.01 | 2.44 | 0.74 | 0.00 | 0.07 | 0.98 | 0.34 | 0.95 | 0.01 | 0.85 |
| Kaohsiung | 16.91 | 1.37 | 0.17 | 1.84 | 0.15 | 1.40 | 1.34 | 3.74 | 0.37 | 0.01 | 0.07 | 6.45 |
| Taipei | 8.90 | 0.84 | 0.06 | 1.10 | 0.05 | 0.07 | 0.70 | 2.47 | 0.18 | 0.02 | 0.02 | 3.39 |
| Norman | 6.20 | 0.37 | 0.00 | 1.09 | 0.00 | 0.00 | 0.28 | 0.73 | 0.08 | 0.00 | 0.00 | 3.64 |
| Pasadena | 6.97 | 0.42 | 0.02 | 0.77 | 0.04 | 0.31 | 0.26 | 1.04 | 0.12 | 0.01 | 0.02 | 3.97 |
| Johannesburg | 16.75 | 2.45 | 0.19 | 1.30 | 0.00 | 0.03 | 1.16 | 3.57 | 0.30 | 0.01 | 0.30 | 7.45 |
| Pretoria | 16.97 | 2.31 | 0.10 | 1.65 | 0.00 | 0.01 | 1.26 | 3.80 | 0.30 | 0.00 | 0.23 | 7.31 |
| Average | 19.40 | 2.04 | 0.45 | 3.69 | 0.10 | 0.43 | 1.02 | 3.50 | 0.35 | 0.18 | 0.26 | 7.38 |

PBW is the calculated water mass at 35% RH. RM indicates residual matter.

Table S5. Distribution of samples through the seasons along with the average $PM_{2.5}$ concentration.

| Site | N | DJF | MAM | JJA | SON | $PM_{2.5}$ concentration |
|---|---|---|---|---|---|---|
| Abu Dhabi | 93 | 23 | 18 | 32 | 20 | 32.93 |
| Melbourne | 47 | 16 | 16 | 5 | 10 | 4.79 |
| Dhaka | 53 | 0 | 6 | 42 | 5 | 37.52 |
| Bujumbura | 37 | 12 | 10 | 14 | 1 | 30.67 |
| Halifax | 91 | 18 | 14 | 22 | 37 | 3.11 |
| Sherbrooke | 61 | 16 | 22 | 16 | 7 | 4.64 |
| Beijing | 197 | 38 | 55 | 49 | 55 | 25.49 |
| Addis Ababa | 162 | 57 | 51 | 28 | 26 | 21.66 |
| Bandung | 14 | 2 | 4 | 8 | 0 | 27.30 |
| Haifa | 142 | 29 | 45 | 37 | 31 | 12.85 |
| Rehovot | 162 | 55 | 29 | 37 | 41 | 14.21 |
| Delhi | 20 | 0 | 20 | 0 | 0 | 55.40 |
| Kanpur | 15 | 3 | 6 | 5 | 1 | 43.88 |
| Seoul | 73 | 20 | 19 | 15 | 19 | 18.14 |
| Ulsan | 96 | 24 | 29 | 24 | 19 | 12.65 |
| Mexico City | 53 | 17 | 20 | 8 | 8 | 15.51 |
| Ilorin | 17 | 6 | 1 | 3 | 7 | 25.63 |
| Fajardo | 54 | 15 | 10 | 13 | 16 | 6.49 |
| Kaohsiung | 139 | 47 | 27 | 33 | 32 | 16.91 |
| Taipei | 241 | 61 | 50 | 66 | 64 | 8.90 |
| Norman | 12 | 4 | 2 | 3 | 3 | 6.20 |
| Pasadena | 246 | 70 | 38 | 75 | 63 | 6.97 |
| Johannesburg | 188 | 40 | 42 | 53 | 53 | 16.75 |
| Pretoria | 230 | 41 | 62 | 67 | 60 | 16.97 |

DJF – number of samples with stop sampling dates occurring in the months of December, January, and February. MAM – number of samples with stop sampling dates occurring in the months of March, April, and May. JJA – number of samples with stop sampling dates occurring in the months of June, July, and August. SON – number of samples with stop sampling dates occurring in the months of September, October, and November.

Table S6. Number of samples (N) obtained from each site along with the date of the first and last sample obtained. The percentage water calculated from the composition for the period and the fraction of water attributable to each growth category are also included.

| Site | First sample Date | Latest sample Date | N | High growth category | Middle growth category | Low growth category | Percent water |
|---|---|---|---|---|---|---|---|
| Abu Dhabi | 7/27/2020 | 9/22/2024 | 93 | 0.108 | 0.882 | 0.010 | 2.274 |
| Melbourne | 8/9/2022 | 5/20/2024 | 47 | 0.558 | 0.313 | 0.129 | 3.108 |
| Dhaka | 8/11/2020 | 6/2/2024 | 53 | 0.267 | 0.549 | 0.184 | 1.535 |
| Bujumbura | 12/9/2022 | 8/9/2024 | 37 | 0.073 | 0.321 | 0.606 | 1.182 |
| Halifax | 1/14/2020 | 2/12/2024 | 91 | 0.420 | 0.375 | 0.205 | 2.551 |
| Sherbrooke | 3/10/2020 | 8/22/2024 | 61 | 0.119 | 0.509 | 0.371 | 1.639 |
| Beijing | 3/24/2020 | 8/18/2024 | 197 | 0.060 | 0.798 | 0.142 | 2.165 |
| Addis Ababa | 12/7/2022 | 5/13/2024 | 162 | 0.094 | 0.539 | 0.367 | 1.072 |
| Bandung | 12/31/2019 | 7/11/2021 | 14 | 0.073 | 0.615 | 0.313 | 1.729 |
| Haifa | 2/16/2022 | 6/17/2023 | 142 | 0.167 | 0.747 | 0.086 | 2.346 |
| Rehovot | 7/2/2020 | 6/7/2023 | 162 | 0.132 | 0.757 | 0.112 | 2.070 |
| Delhi | 3/5/2024 | 5/13/2024 | 20 | 0.395 | 0.424 | 0.181 | 2.189 |
| Kanpur | 7/14/2021 | 5/24/2022 | 15 | 0.088 | 0.672 | 0.240 | 1.537 |
| Seoul | 9/11/2020 | 1/8/2024 | 73 | 0.039 | 0.761 | 0.200 | 1.995 |
| Ulsan | 10/28/2021 | 8/22/2024 | 96 | 0.155 | 0.666 | 0.179 | 2.131 |
| Mexico City | 2/26/2021 | 6/9/2024 | 53 | 0.037 | 0.689 | 0.274 | 1.710 |
| Ilorin | 6/22/2020 | 12/1/2021 | 17 | 0.215 | 0.434 | 0.352 | 0.851 |
| Fajardo | 3/18/2021 | 2/7/2024 | 54 | 0.820 | 0.162 | 0.019 | 5.470 |
| Kaohsiung | 8/20/2022 | 7/26/2024 | 139 | 0.162 | 0.687 | 0.150 | 2.350 |
| Taipei | 1/27/2022 | 8/4/2024 | 241 | 0.206 | 0.658 | 0.136 | 2.408 |
| Norman | 6/28/2023 | 3/18/2024 | 12 | 0.061 | 0.541 | 0.398 | 1.419 |
| Pasadena | 11/9/2021 | 8/23/2024 | 246 | 0.234 | 0.524 | 0.241 | 2.110 |
| Johannesburg | 4/10/2022 | 7/26/2024 | 188 | 0.057 | 0.697 | 0.246 | 1.785 |
| Pretoria | 10/22/2020 | 7/1/2024 | 230 | 0.065 | 0.703 | 0.231 | 1.824 |
| Average | | | | 0.192 | 0.584 | 0.224 | 2.060 |

## References


Dillner, A. and Takahama, S.: Predicting ambient aerosol thermal-optical reflectance measurements from infrared spectra: elemental carbon, Atmos. Meas. Tech., 8, 4013–4023, 10.5194/amt-8-4013-2015, 2015a.

Dillner, A. and Takahama, S.: Predicting ambient aerosol thermal-optical reflectance (TOR) measurements from infrared spectra: organic carbon, Atmos. Meas. Tech., 8, 1097–1109, 10.5194/amt-8-1097-2015, 2015b.

Donahue, N., Robinson, A., Stanier, C., and Pandis, S.: Coupled partitioning, dilution, and chemical aging of semivolatile organics, Environ. Sci. Technol., 40, 2635–2643, 10.1021/es052297c, 2006.

McInnes, L. M., Quinn, P. K., Covert, D. S., and Anderson, T. L.: Gravimetric analysis, ionic composition, and associated water mass of the marine aerosol, Atmos. Environ., 30, 869–884, 10.1016/1352-2310(95)00354-1, 1996.

Pandey, A., Shetty, N., and Chakrabarty, R.: Aerosol light absorption from optical measurements of PTFE membrane filter samples: sensitivity analysis of optical depth measures, Atmos. Meas. Tech., 12, 1365–1373, 10.5194/amt-12-1365-2019, 2019.

Reggente, M., Dillner, A., and Takahama, S.: Predicting ambient aerosol thermal-optical reflectance (TOR) measurements from infrared spectra: extending the predictions to different years and different sites, Atmos. Meas. Tech., 9, 441–454, 10.5194/amt-9-441-2016, 2016.

Zhong, M. and Jang, M.: Light absorption coefficient measurement of SOA using a UV-Visible spectrometer connected with an integrating sphere, Atmos. Environ., 45, 4263–4271, 10.1016/j.atmosenv.2011.04.082, 2011.